PHYSICAL REVIEW D **88,** 052002 (2013)

Measurement of the polarization amplitudes in $B^0 \to J/\psi K^*(892)^0$ decays

R. Aaij *et al.**
(LHCb Collaboration)

(Received 11 July 2013; published 3 September 2013)

An analysis of the decay $B^0 \to J/\psi K^*(892)^0$ is presented using data, corresponding to an integrated luminosity of 1.0 fb^{-1}, collected in pp collisions at a center-of-mass energy of 7 TeV with the LHCb detector. The polarization amplitudes and the corresponding phases are measured to be $|A_\parallel|^2 = 0.227 \pm 0.004\,(\text{stat}) \pm 0.011\,(\text{syst})$, $|A_\perp|^2 = 0.201 \pm 0.004\,(\text{stat}) \pm 0.008\,(\text{syst})$, $\delta_\parallel[\text{rad}] = -2.94 \pm 0.02\,(\text{stat}) \pm 0.03\,(\text{syst})$, and $\delta_\perp[\text{rad}] = 2.94 \pm 0.02\,(\text{stat}) \pm 0.02\,(\text{syst})$. Comparing $B^0 \to J/\psi K^*(892)^0$ and $\bar{B}^0 \to J/\psi \bar{K}^*(892)^0$ decays, no evidence for direct CP violation is found.

DOI: 10.1103/PhysRevD.88.052002 PACS numbers: 13.25.Hw, 13.25.−k, 13.88.+e

I. INTRODUCTION

The measurement of the polarization content of the decay $B^0 \to J/\psi(\mu^+\mu^-)K^{*0}(K^+\pi^-)$ and its charge-conjugate $\bar{B}^0 \to J/\psi(\mu^+\mu^-)\bar{K}^{*0}(K^-\pi^+)$ is presented in this paper, where the notation K^{*0} is used to refer to the $K^*(892)^0$ meson. Recent measurements have been erformed by *BABAR* (2007 [1]), Belle (2005 [2]), and CDF (2005 [3]). A detailed comparison can be found in Sec. VII. The decay can be decomposed in terms of three transversity states, corresponding to the relative orientation of the linear polarization vectors of the two vector mesons. The amplitudes are referred to as P-wave amplitudes since the $K\pi$ system is in a P-wave state and are denoted by A_0 (longitudinal), $A_\parallel$ (transverse-parallel), and $A_\perp$ (transverse-perpendicular), where the relative orientations are shown in parentheses. An additional S-wave amplitude corresponding to a nonresonant $K\pi$ system is denoted by A_S. The strong phases of the four amplitudes are δ_0, $\delta_\parallel$, $\delta_\perp$, and δ_S, respectively, and by convention δ_0 is set to zero. The parity of the final states is even for A_0 and $A_\parallel$, and odd for $A_\perp$ and A_S.

The Standard Model (SM) predicts that the $B^0 \to J/\psi(\mu^+\mu^-)K^{*0}(K^+\pi^-)$ decay is dominated by a color-suppressed tree diagram [Fig. 1(a)], with highly suppressed contributions from gluonic and electroweak loop (penguin) diagrams [Fig. 1(b)]. Neglecting the penguin contributions and using naïve factorization for the tree diagram leads to predictions for the P-wave amplitudes $|A_0|^2 \approx 0.5$ and $A_\parallel \approx A_\perp$ [4]. In the absence of final state interactions, the phases $\delta_\parallel$ and $\delta_\perp$ are both predicted to be 0 or π rad. Corrections of order 5% to these predictions from QCD have been incorporated in more recent calculations [5,6].

The signal decay is flavor specific, with $K^{*0} \to K^+\pi^-$ or $\bar{K}^{*0} \to K^-\pi^+$ indicating a B^0 or $\bar{B}^0$ decay, respectively. In the SM, the amplitudes for the decay and its charge conjugate are equal, but in the presence of physics beyond the SM (BSM) the loop contributions could be enhanced and introduce CP-violating differences between the B^0 and $\bar{B}^0$ decay amplitudes [7–9]. An analysis of the angular distributions of the decay products gives increased sensitivity to BSM physics through differences in the individual amplitudes [10].

A further motivation for studying $B^0 \to J/\psi K^{*0}$ decays is that the magnitudes and phases of the amplitudes should be approximately equal to those in $B_s^0 \to J/\psi\phi$ decays [11]. Both decay modes are dominated by color-suppressed tree diagrams and have similar branching fractions, $\mathcal{B}(B^0 \to J/\psi K^{*0}) = (1.29 \pm 0.14) \times 10^{-3}$ [12] (S-wave subtracted) and $\mathcal{B}(B_s^0 \to J/\psi\phi) = (1.05 \pm 0.11) \times 10^{-3}$ [13]. Any BSM effects observed in $B^0 \to J/\psi K^{*0}$ may also be present in $B_s^0 \to J/\psi\phi$, where they would modify the time-dependent CP violation and the CP-violating phase ϕ_s [14].

II. ANGULAR ANALYSIS

To measure the individual polarization amplitudes $(A_0, A_\parallel, A_\perp, A_S)$ the decay is analyzed in terms of three angular variables, denoted as $\Omega = \{\cos\theta, \cos\psi, \varphi\}$ in the transversity basis (Fig. 2). For a B^0 decay, the angle between the μ^+ momentum direction and the z axis in the J/ψ rest frame is denoted θ, and φ is the azimuthal angle of the μ^+ momentum direction in the same frame. ψ is the angle between the momentum direction of the K^+ meson and the negative momentum direction of the J/ψ meson in the $K^{*0} \to K^+\pi^-$ rest frame. For $\bar{B}^0$ decays, the angles are defined with respect to the μ^- and the K^- meson.

In this analysis the flavor of the B meson at production is not measured. Therefore, the observed $B^0 \to J/\psi K^{*0}$ decays arise from both initial B^0 or $\bar{B}^0$ mesons as a result of oscillations. Summing over both contributions, the differential decay rate can be written as [15,16]

$$\frac{d^4\Gamma(B^0 \to J/\psi K^{*0})}{dt\,d\Omega} \propto e^{-\Gamma_d t} \sum_{k=1}^{10} h_k f_k(\Omega), \qquad (1)$$

*Full author list given at the end of the article.

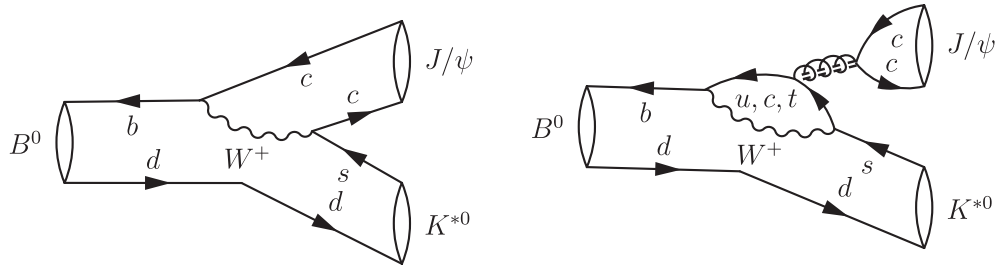

(a) Tree (b) Penguin

FIG. 1. Feynman diagrams contributing to $B^0 \to J/\psi K^{*0}$ decays.

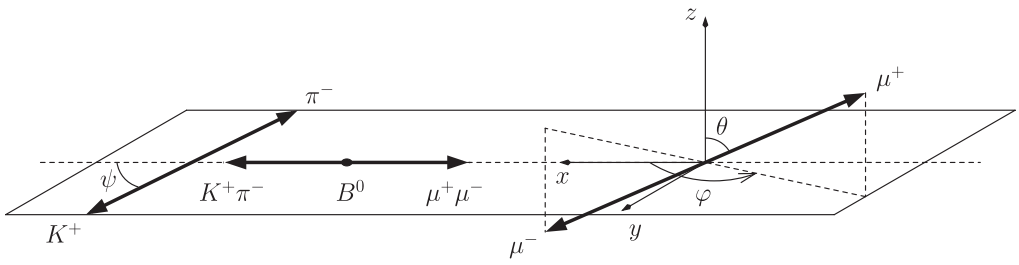

FIG. 2. Definitions of the transversity angles θ, ψ, φ, as described in the text.

where t is the decay time and Γ_d is the total decay width of the B^0 meson; h_k are combinations of the polarization amplitudes and f_k are functions of the three transversity angles. These factors can be found in Table I. The h_k combinations are invariant under the phase transformation $(\delta_\parallel, \delta_\perp, \delta_S) \leftrightarrow (-\delta_\parallel, \pi - \delta_\perp, -\delta_S)$. This twofold ambiguity can be resolved by measuring the phase difference between the S- and P-wave amplitudes as a function of $m(K^+\pi^-)$ (see Sec. VII). The difference in decay width between the heavy and light eigenstates, $\Delta\Gamma_d$, has been neglected.

The differential decay rate for $\bar{B}^0 \to J/\psi \bar{K}^{*0}$ is obtained from Eq. (1) by defining the angles using the charge conjugate final state particles and multiplying the interference terms f_4, f_6, and f_9 in Table I by -1. To allow for possible direct CP violation, the amplitudes are changed from A_i to $\bar{A}_i$ ($i = 0, \parallel, \perp, S$).

TABLE I. Definition of h_k and f_k appearing in Eq. (1). The h_k factors are invariant under the phase transformation $(\delta_\parallel, \delta_\perp, \delta_S) \longleftrightarrow (-\delta_\parallel, \pi - \delta_\perp, -\delta_S)$ [15,16]. f_k are functions defined such that their integrals over Ω are unity.

k	h_k	$f_k(\Omega)$
1	$\lvert A_0\rvert^2$	$\frac{9}{32\pi} 2\cos^2\psi(1 - \sin^2\theta\cos^2\varphi)$
2	$\lvert A_\parallel\rvert^2$	$\frac{9}{32\pi}\sin^2\psi(1 - \sin^2\theta\sin^2\varphi)$
3	$\lvert A_\perp\rvert^2$	$\frac{9}{32\pi}\sin^2\psi\sin^2\theta$
4	$\lvert A_\parallel\rvert\lvert A_\perp\rvert\sin(\delta_\perp - \delta_\parallel)$	$-\frac{9}{32\pi}\sin^2\psi\,\sin 2\theta\,\sin\varphi$
5	$\lvert A_0\rvert\lvert A_\parallel\rvert\cos(\delta_\parallel)$	$\frac{9}{32\pi\sqrt{2}}\sin 2\psi\sin^2\theta\,\sin 2\varphi$
6	$\lvert A_0\rvert\lvert A_\perp\rvert\sin(\delta_\perp)$	$\frac{9}{32\pi\sqrt{2}}\sin 2\psi\,\sin 2\theta\cos\varphi$
7	$\lvert A_S\rvert^2$	$\frac{3}{32\pi} 2(1 - \sin^2\theta\cos^2\varphi)$
8	$\lvert A_\parallel\rvert\lvert A_S\rvert\cos(\delta_\parallel - \delta_S)$	$\frac{3}{32\pi}\sqrt{6}\sin\psi\sin^2\theta\,\sin 2\varphi$
9	$\lvert A_\perp\rvert\lvert A_S\rvert\sin(\delta_\perp - \delta_S)$	$\frac{3}{32\pi}\sqrt{6}\sin\psi\,\sin 2\theta\cos\varphi$
10	$\lvert A_0\rvert\lvert A_S\rvert\cos(\delta_S)$	$\frac{3}{32\pi} 4\sqrt{3}\cos\psi(1 - \sin^2\theta\cos^2\varphi)$

III. LHCb DETECTOR

The LHCb detector [17] is a single-arm forward spectrometer covering the pseudorapidity range $2 < \eta < 5$, designed for the study of particles containing b or c quarks. The detector includes a high-precision tracking system consisting of a silicon-strip vertex detector surrounding the pp interaction region, a large-area silicon-strip detector located upstream of a dipole magnet with a bending power of about 4 Tm, and three stations of silicon-strip detectors and straw drift tubes placed downstream. The combined tracking system provides a momentum measurement with relative uncertainty that varies from 0.4% at 5 GeV/c to 0.6% at 100 GeV/c, and impact parameter resolution of 20 μm for tracks with high transverse momentum (p_T). Different types of charged hadrons are distinguished by information from two ring-imaging Cherenkov detectors [18]. Photon, electron, and hadron candidates are identified by a calorimeter system consisting of scintillating-pad and preshower detectors, an electromagnetic calorimeter, and a hadronic calorimeter. Muons are identified by a system composed of alternating layers of iron and multiwire proportional chambers. The trigger consists of a hardware stage, based on information from the calorimeter and muon systems, followed by a software stage, which applies a full event reconstruction. In the simulation, pp collisions are generated using PYTHIA 6.4 [19] with a specific LHCb

configuration [20]. Decays of hadronic particles are described by EVTGEN [21], in which final state radiation is generated using PHOTOS [22]. The interaction of the generated particles with the detector and its response are implemented using the GEANT4 toolkit [23] as described in Ref. [24].

IV. DATA SAMPLES AND CANDIDATE SELECTION

In the following $B^0 \to J/\psi K^{*0}$ refers to both charge-conjugate decays unless otherwise stated. The selection of $B^0 \to J/\psi K^{*0}$ candidates is based upon the decays of the $J/\psi \to \mu^+\mu^-$ and the $K^{*0} \to K^+\pi^-$ final states. Candidates must satisfy the hardware trigger [25], which selects events containing muon candidates that have high transverse momentum with respect to the beam direction. The subsequent software trigger [25] is composed of two stages. The first stage performs a partial event reconstruction and requires events to have two well-identified oppositely charged muons with invariant mass larger than 2.7 GeV/c^2. The second stage of the software trigger performs a full event reconstruction and only retains events containing a $\mu^+\mu^-$ pair that has invariant mass within 120 MeV/c^2 of the known J/ψ mass [26] and forms a vertex that is significantly displaced from the nearest primary pp interaction vertex (PV).

The J/ψ candidates are formed from two oppositely charged tracks, being identified as muons, having $p_T >$ 500 MeV/c and originating from a common vertex. The invariant mass of this pair of muons must be in the range 3030–3150 MeV/c^2.

The K^{*0} candidates are formed from two oppositely charged tracks, one identified as a kaon and one as a pion, which originate from the same vertex. It is required that the K^{*0} candidate has $p_T > 2$ GeV/c and invariant mass in the range 826–966 MeV/c^2.

The B^0 candidates are reconstructed from the J/ψ and K^{*0} candidates, with the invariant mass of the $\mu^+\mu^-$ pair constrained to the known J/ψ mass. The resulting B^0 candidates are required to have an invariant mass $m(J/\psi K^+\pi^-)$ in the range 5150–5400 MeV/c^2. The decay time of the B^0 candidate is calculated from a vertex and kinematic fit that constrains the B^0 candidate to originate from its associated PV [27]. The χ^2 per degree of freedom of the fit is required to be less than 5. For events with multiple B^0 candidates, the candidate with the smallest fit χ^2 per degree of freedom is chosen. Only B^0 candidates with a decay time in the range 0.3–14 ps are retained. The lower bound on the decay time rejects a large fraction of the prompt combinatorial background.

In the data sample, corresponding to an integrated luminosity of 1.0 fb^{-1}, collected in pp collisions at a center-of-mass energy of 7 TeV with the LHCb detector, a total of 77 282 candidates are selected. The invariant mass distribution is shown in Fig. 3. From a fit the number of signal decays is found to be 61 244 ± 132. The uncertainties on the signal yields quoted here and in Sec. VII come from propagating the uncertainty on the signal fraction evaluated by the fit.

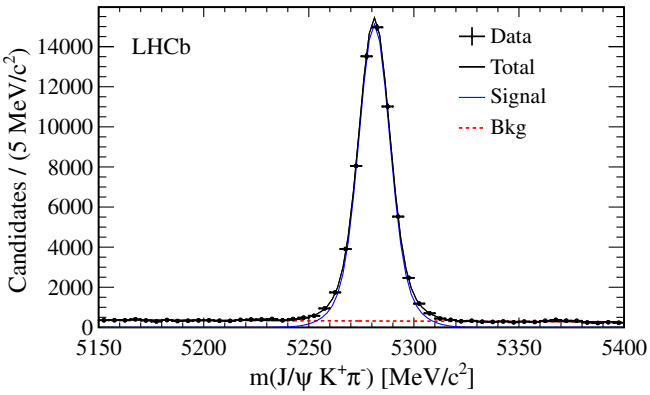

FIG. 3 (color online). Invariant mass distribution of the selected $B^0 \to J/\psi K^{*0}$ candidates. The curves for the signal (solid blue line), background (dashed red line), and total (solid black line) as determined from a fit are shown.

V. MAXIMUM LIKELIHOOD FIT

The parameters used in this analysis are $|A_\parallel|^2$, $|A_\perp|^2$, F_S, $\delta_\parallel$, $\delta_\perp$, and δ_S, where we introduce the parameter $F_S = |A_S|^2/(1 + |A_S|^2)$ to denote the fractional S-wave component. The parameter $|A_0|^2$ is determined by the constraint $|A_0|^2 + |A_\parallel|^2 + |A_\perp|^2 = 1$. The best fit values of these parameters are determined with an unbinned maximum log-likelihood fit to the decay time and angular distributions of the selected B^0 candidates. To subtract the background component, each event is given a signal weight, W_i, using the *sPlot* [28] method with $m(J/\psi K^+\pi^-)$ as the discriminating variable. The invariant mass distribution of the signal is modeled as the sum of two Gaussian functions with a common mean. The mean and widths of both Gaussian functions, as well as the fraction of the first Gaussian are parameters determined by the fit. The effective resolution of the mass peak is determined to be 9.3 ± 0.8 MeV/c^2. The invariant mass distribution of the background is described by an exponential function. The signal fraction in a ±30 MeV/c window around the known B^0 mass [26] is approximately 93%.

A maximum likelihood fit is then performed with each candidate weighted by W_i. The fit uses a signal-only probability density function (PDF), which is denoted $\mathcal{S}$. It is a function of the decay time t and angles Ω, and is obtained from Eq. (1). The exponential decay time function is convolved with a Gaussian function to take into account the decay time resolution of 45 fs [14]. The effect of the time and angular resolution on this analysis has been studied and found to be negligible [16].

The fit minimizes the negative log-likelihood summed over the selected candidates

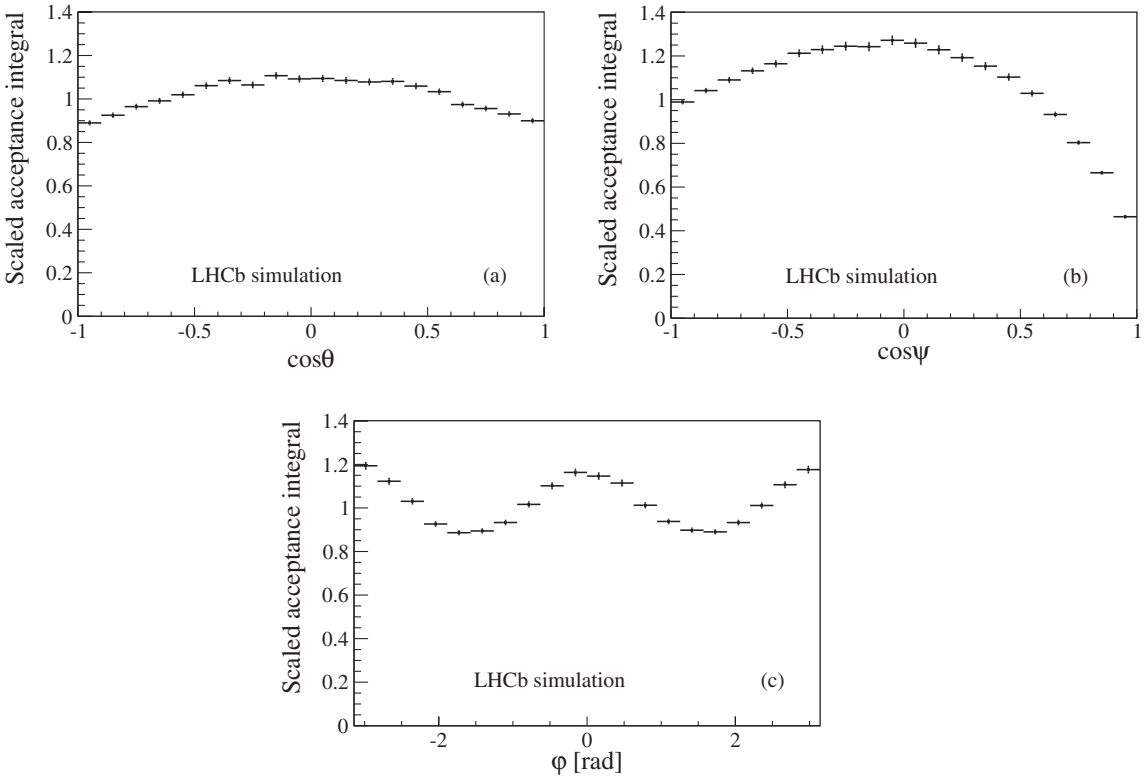

FIG. 4. Angular acceptance $A(\Omega)$ as a function of each decay angle, integrated over the other two angles for (a) $\cos\theta$, (b) $\cos\psi$, and (c) φ. The projections are normalized such that their average value over the histogram range is unity.

$$-\ln\mathcal{L} = -\alpha\sum_i W_i \ln\mathcal{S}_i(t_i, \Omega_i), \tag{2}$$

where $\alpha = \sum_i W_i / \sum_i W_i^2$ is a normalization factor accounting for the effect of the weights in the determination of the uncertainties [29].

The selection applied to the data is almost unbiased with respect to the decay time. The measurements of amplitudes and phases are insensitive to the decay time acceptance since $\Delta\Gamma_d \sim 0$ and the time dependence of the PDF factorizes out from the angular part. Nevertheless, the small deviation of the decay time acceptance from uniformity is determined from data using decay time unbiased triggers as a reference and is included in the fitting procedure.

The acceptance as a function of the decay angles is not uniform because of the forward geometry of the detector and the momentum selection requirements applied to the final state particles. A three-dimensional acceptance function, $A(\Omega)$, is determined using simulated events subject to the same selection criteria as the data and is included in the fit. Figure 4 shows the acceptance as a function of each decay angle, integrated over the two other angles. The variation in acceptance is asymmetric for $\cos\psi$, due to the selection requirements on the π^- and the K^{*0} mesons.

The phase of the P-wave amplitude increases rapidly as a function of the $K^+\pi^-$ invariant mass, whereas the S-wave phase increases relatively slowly [30]. As a result the phase difference between the S- and P-wave amplitudes falls with increasing $K^+\pi^-$ invariant mass. A fit that determines the phase difference in bins of $m(K^+\pi^-)$ can therefore be used to select the physical solution and hence resolve the ambiguity described in Sec. II. This method has previously been used to measure the sign of $\Delta\Gamma_s$ in the B_s^0 system [31]. In the analysis the data are divided into four bins of $m(K^+\pi^-)$, shown in Fig. 5 and defined in Table II. A simultaneous fit to all four bins is performed in which the

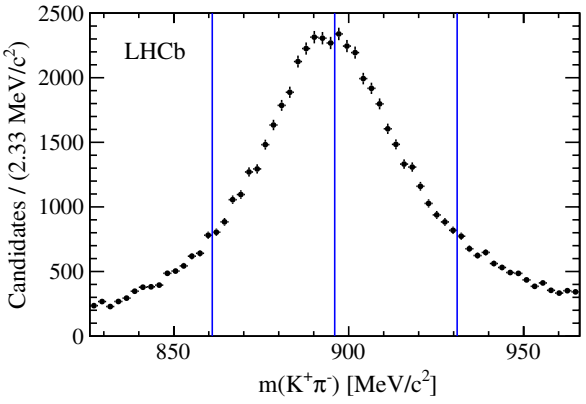

FIG. 5 (color online). Background subtracted distribution of the $m(K^+\pi^-)$ invariant mass. The four bins used to resolve the ambiguity in the strong phases are shown.

TABLE II. Bins of $m(K^+\pi^-)$ and the corresponding C_{SP} correction factor for the S-wave interference terms, assuming a uniform distribution for the nonresonant $K^+\pi^-$ contribution and a relativistic Breit-Wigner shape for decays via the K^{*0} resonance.

$m(K^+\pi^-)$ [MeV/c^2]	C_{SP}
826–861	0.984
861–896	0.946
896–931	0.948
931–966	0.985

P-wave parameters are common, but F_S and δ_S are independent parameters in each bin. Consistent results are obtained with the use of two or six bins.

To correct for the variation of the S-wave relative to the P-wave over the $m(K^+\pi^-)$ range of each bin, a correction factor is introduced in each of the three interference terms f_8, f_9, and f_{10} in Eq. (1). The S-wave line shape is assumed to be uniform across the $m(K^+\pi^-)$ range, and the P-wave shape is described by a relativistic Breit-Wigner function. The correction factor is calculated by integrating the product ps^*

$$\int_{m^L_{K^+\pi^-}}^{m^H_{K^+\pi^-}} ps^* dm(K^+\pi^-) = C_{SP} e^{-i\theta_{SP}}, \quad (3)$$

where p and s are the P- and S-wave line shapes normalized to unity in the range of integration, * is the complex conjugation operator, $m^L_{K^+\pi^-}$ and $m^H_{K^+\pi^-}$ denote the boundaries of the $m(K^+\pi^-)$ bin, C_{SP} is the correction factor, and θ_{SP} is absorbed in the measurements of $\delta_S - \delta_0$. The C_{SP} factors tend to unity (i.e. no correction) as the bin width tends to zero. The C_{SP} factors calculated for this analysis are given in Table II. The factors are close to unity, and hence the analysis is largely insensitive to this correction.

VI. SYSTEMATIC UNCERTAINTIES

To estimate the systematic uncertainties arising from the choice of the model for the B^0 invariant mass, the signal mass PDF is changed from a double Gaussian function to either a single Gaussian or a crystal ball function. The largest differences observed in the fitted values of the parameters are assigned as systematic uncertainties.

To account for uncertainties in the treatment of the combinatorial background, an alternative fit to the data is performed without using signal weights. An explicit background model, $\mathcal{B}$, is constructed, with the time distribution being described by two exponential functions, and the angular distribution by a three-dimensional histogram derived from the sidebands of the B^0 invariant mass distribution. A fit is then made to the unweighted data sample with the sum of $\mathcal{S}$ and $\mathcal{B}$. The results of this fit are consistent with those from the fit using signal weights, and the small differences are included as systematic uncertainties.

A very small contribution from the decay $B^0_s \to J/\psi \bar{K}^{*0}$ [32] in the high-mass sideband of the B^0 invariant mass distribution of Fig. 3 has a negligible effect on the fit results. The only significant background that peaks in the B^0 mass region arises from candidates where one or more of the tracks are misreconstructed, in most of the

TABLE III. Systematic uncertainties as described in the text. The contribution from omitting the C_{SP} factors is negligible for the P-wave parameters. The total systematic uncertainty is the sum in quadrature of the individual contributions.

(a) P-wave parameters

Source	$\lvert A_\parallel\rvert^2$	$\lvert A_\perp\rvert^2$	$\delta_\parallel$ [rad]	$\delta_\perp$ [rad]
Mass model	0.000	0.001	0.00	0.00
Background treatment	0.002	0.001	0.00	0.00
Misreconstructed background	0.002	0.000	0.00	0.01
Angular acceptance	0.009	0.007	0.03	0.01
Statistical uncertainty on acceptance	0.001	0.001	0.01	0.01
Other resonances	0.005	0.004	0.00	0.01
Total systematic uncertainty	0.011	0.008	0.03	0.02
Statistical uncertainty	0.004	0.004	0.02	0.02

(b) S-wave parameters of bins (1) and (2)

Source	$F_S^{(1)}$	$\delta_S^{(1)}$ [rad]	$F_S^{(2)}$	$\delta_S^{(2)}$ [rad]
Mass model	0.005	0.01	0.001	0.01
Background treatment	0.003	0.04	0.001	0.01
Misreconstructed background	0.006	0.01	0.002	0.00
Angular acceptance	0.007	0.01	0.004	0.05
Statistical uncertainty on acceptance	0.003	0.04	0.002	0.03
C_{SP} factors	0.003	0.00	0.005	0.01
Other resonances	0.016	0.06	0.002	0.02
Total systematic uncertainty	0.020	0.08	0.007	0.06
Statistical uncertainty	0.007	0.10	0.004	0.06

(c) S-wave parameters of bins (3) and (4)

Source	$F_S^{(3)}$	$\delta_S^{(3)}$ [rad]	$F_S^{(4)}$	$\delta_S^{(4)}$ [rad]
Mass model	0.003	0.01	0.004	0.01
Background treatment	0.001	0.01	0.003	0.02
Misreconstructed background	0.003	0.01	0.004	0.01
Angular acceptance	0.000	0.08	0.003	0.05
Statistical uncertainty on acceptance	0.002	0.03	0.003	0.04
C_{SP} factors	0.005	0.00	0.002	0.00
Other resonances	0.006	0.02	0.000	0.08
Total systematic uncertainty	0.009	0.09	0.008	0.11
Statistical uncertainty	0.006	0.03	0.014	0.03

TABLE IV. Results for $B^0 \to J/\psi K^{*0}$ candidates. The uncertainties are statistical and systematic, respectively.

Parameter	Value
$\lvert A_\parallel \rvert^2$	$0.227 \pm 0.004 \pm 0.011$
$\lvert A_\perp \rvert^2$	$0.201 \pm 0.004 \pm 0.008$
$\delta_\parallel$ [rad]	$-2.94 \pm 0.02 \pm 0.03$
$\delta_\perp$ [rad]	$2.94 \pm 0.02 \pm 0.02$

cases the pion track. From simulation studies we find that this corresponds to 3.5% of the signal yield and has a similar B^0 mass distribution to the signal but a significantly different angular distribution. The yield and shape of the background are taken from simulated events and are used to explicitly model this background in the data fit. The effect on the fit results is taken as a systematic uncertainty. Other background contributions are found to be insignificant.

The angular acceptance function is determined from simulated events, and a systematic uncertainty is included to take into account the limited size of the simulated event sample. An observed difference in the kinematic distributions of the final state particles between data and simulation is largely attributed to the S-wave component, which is not included in the simulation. To account for the S-wave, the simulated events are reweighted to match the signal distributions expected from the best estimate of the physics parameters from data (including the S-wave). After this procedure, small differences remain in the pion and kaon momentum distributions. The simulated events are further reweighted to remove these differences, and the change in the fit results is taken as the systematic uncertainty due to the modeling of the acceptance.

The $C_{\rm SP}$ factors do not affect the P-wave amplitudes and have only a small effect on the S-wave amplitudes. The fit is performed with each $C_{\rm SP}$ factor set to unity, and the differences in the S-wave parameters are taken as a systematic uncertainty.

This analysis assumes only P- and S-wave contributions to the $K^+\pi^-$ system, but makes no assumption about the $m(K^+\pi^-)$ mass model itself (except in the determination of the $C_{\rm SP}$ factors). The S-wave fractions reported in Table V correspond to a shape that does not exhibit an approximately linear S-wave (as might be naïvely expected). A separate study of the $m(K^+\pi^-)$ mass spectrum and angular distribution has been performed over a wider $m(K^+\pi^-)$ mass range. This study indicates that there may be contributions from additional resonances, e.g. $\kappa(800)$, $K^*(1410)$, $K_2^*(1430)$, and $K^*(1680)$ states. Of particular interest is the $K_2^*(1430)$ contribution, which is a D-wave state and can interfere with the P-wave. Using simulated pseudoexperiments such interferences are observed to change the shape of the observed $m(K^+\pi^-)$ spectrum

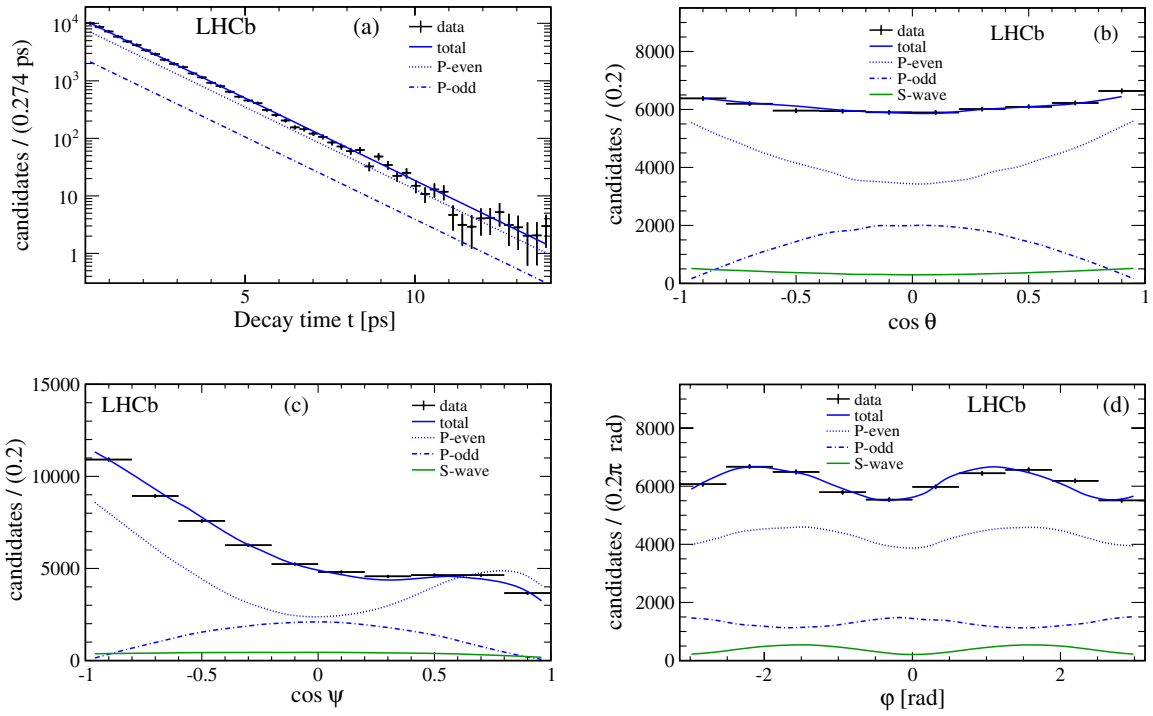

FIG. 6 (color online). Projections of (a) the decay time and the transversity angles (b) $\cos\theta$, (c) $\cos\psi$, and (d) φ from the fit to the data (points with statistical error bars). The different curves show the P-wave parity-even (dotted blue lines) and parity-odd (dashed blue lines) components, the pure S-wave (green lines) contributions without interference, as well as the total signal component (solid blue lines).

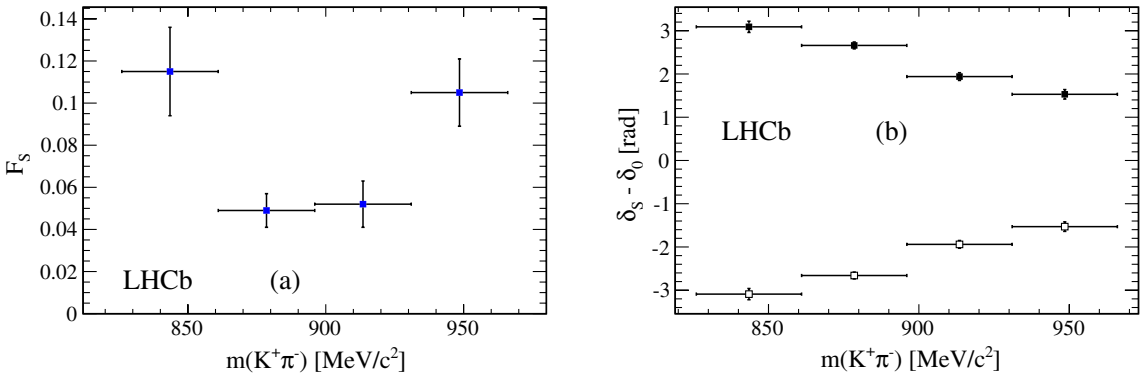

FIG. 7 (color online). Variation of (a) F_S and (b) $\delta_S - \delta_0$ in the simultaneous fit in four bins of the $K^+\pi^-$ mass. There are two solutions of the relative phase, the falling trend (solid points) being the physical one.

from that corresponding to a simple linear S-wave, and that by ignoring such possible additional resonances the P- and S-wave parameters may be biased. These biases are estimated using simulated experiments containing these additional resonances, and they are assigned as systematic uncertainties. The systematic uncertainties are summarized in Table III.

VII. RESULTS

The values of the P-wave parameters obtained from the fit to the combined $B^0 \to J/\psi K^{*0}$ and $\bar{B}^0 \to J/\psi \bar{K}^{*0}$ samples, assuming no direct CP violation, are shown in Table IV with their statistical and systematic uncertainties. The projections of the decay time and the transversity angles are shown in Fig. 6. Although we have included the decay time distribution in the fit, we do not report a lifetime measurement here, which will instead be included in a forthcoming publication. Figure 7 shows the values for F_S and $\delta_S - \delta_0$ as a function of the $K^+\pi^-$ mass. The phase $\delta_0 = 0$ is inserted explicitly to emphasize that this is the phase difference between the S-wave and P-wave. The error bars include both the statistical and the systematic uncertainties. The solid points of Fig. 7(b) correspond to the physical solution with a decreasing phase difference. Table V presents the values of F_S and $\delta_S - \delta_0$ for the physical solution. The correlation matrix for the P- and S-wave parameters is shown in Table VI. Integrating the S-wave fraction over all four $m(K^+\pi^-)$ bins gives an average value of $F_S = (6.4 \pm 0.3 \pm 1.0)\%$ in the full window of ± 70 MeV/c^2 around the known K^{*0} mass [26]. The *BABAR* Collaboration [1] measured an S-wave component of $(7.3 \pm 1.8)\%$ in $B^0 \to J/\psi K^+\pi^-$ in a $K^+\pi^-$ mass range from 0.8 to 1.0 GeV/c^2.

The results of separate fits to $30\,896 \pm 95$ $B^0 \to J/\psi K^{*0}$ and $30\,442 \pm 92$ $\bar{B}^0 \to J/\psi \bar{K}^{*0}$ background subtracted candidates are shown in Table VII, along with the direct CP asymmetries. Only the P-wave amplitudes are allowed to vary in the fit; the S-wave parameters in each $m(K^+\pi^-)$ bin are fixed to the values determined with the combined fit. The fit allows for a difference between the angular acceptance due to charge asymmetries in the detector. The systematic uncertainties are calculated similarly as described in Sec. VI; the uncertainty due to the angular acceptance partially cancels in the direct CP asymmetry calculation. The B^0 and $\bar{B}^0$ fit results are consistent within uncertainties, with the largest difference being approximately 2 standard deviations in $|A_\perp|^2$. There is no evidence for BSM contributions to direct CP violation at the current level of precision.

In previous analyses of the $B^0 \to J/\psi K^{*0}$ polarization amplitudes and phases fits have been performed using a

TABLE V. Signal yield (N_{sig}) and results for the S-wave parameters in each bin of $m(K^+\pi^-)$ mass, showing statistical and systematic uncertainties. Only the physical solution is shown for $\delta_S - \delta_0$.

$m(K^+\pi^-)$ [MeV/c^2]	N_{sig}	Parameter	Value
826–861	$6\,456 \pm 69$	F_S	$0.115 \pm 0.007 \pm 0.020$
		$\delta_S - \delta_0$ [rad]	$3.09 \pm 0.10 \pm 0.08$
861–896	$24\,418 \pm 80$	F_S	$0.049 \pm 0.004 \pm 0.007$
		$\delta_S - \delta_0$ [rad]	$2.66 \pm 0.06 \pm 0.06$
896–931	$23\,036 \pm 77$	F_S	$0.052 \pm 0.006 \pm 0.009$
		$\delta_S - \delta_0$ [rad]	$1.94 \pm 0.03 \pm 0.09$
931–966	$7\,383 \pm 64$	F_S	$0.105 \pm 0.014 \pm 0.008$
		$\delta_S - \delta_0$ [rad]	$1.53 \pm 0.03 \pm 0.11$

TABLE VI. Correlation matrix for the four-bin fit.

	$\lvert A_\parallel\rvert^2$	$\lvert A_\perp\rvert^2$	$\delta_\parallel$	$\delta_\perp$	$F_S(1)$	$\delta_S(1)$	$F_S(2)$	$\delta_S(2)$	$F_S(3)$	$\delta_S(3)$	$F_S(4)$	$\delta_S(4)$
$\lvert A_\parallel\rvert^2$	1.00	−0.70	0.12	0.04	0.02	−0.02	0.10	−0.08	0.14	−0.07	0.10	0.03
$\lvert A_\perp\rvert^2$		1.00	−0.14	−0.01	0.01	0.02	−0.09	0.12	−0.19	0.15	−0.15	−0.01
$\delta_\parallel$			1.00	0.64	−0.01	0.06	−0.06	0.10	−0.07	0.12	−0.02	0.07
$\delta_\perp$				1.00	−0.03	0.14	−0.16	0.21	−0.17	0.18	−0.09	0.05
$F_S(1)$					1.00	−0.24	0.01	−0.01	⋯	⋯	⋯	⋯
$\delta_S(1)$						1.00	−0.03	0.03	−0.03	0.03	−0.02	⋯
$F_S(2)$							1.00	−0.76	0.05	−0.04	0.03	⋯
$\delta_S(2)$								1.00	−0.06	0.05	−0.04	0.01
$F_S(3)$									1.00	−0.59	0.04	⋯
$\delta_S(3)$										1.00	−0.04	0.01
$F_S(4)$											1.00	0.19
$\delta_S(4)$												1.00

TABLE VII. Results from fits to the $B^0 \to J/\psi K^{*0}$ and $\bar{B}^0 \to J/\psi \bar{K}^{*0}$ background subtracted candidates and the direct CP asymmetries $\frac{\bar{X}-X}{\bar{X}+X}$, where X represents the parameter in question. The uncertainties are statistical for the amplitudes and phases and both statistical and systematic for the direct CP measurements.

Parameter	Value for B^0	Value for $\bar{B}^0$	$B^0 - \bar{B}^0$ asymmetry
$\lvert A_\parallel\rvert^2$	0.230 ± 0.005	0.225 ± 0.005	−0.011 ± 0.016 ± 0.005
$\lvert A_\perp\rvert^2$	0.194 ± 0.005	0.207 ± 0.005	0.032 ± 0.018 ± 0.003
$\delta_\parallel$ [rad]	−2.94 ± 0.03	−2.92 ± 0.03	0.003 ± 0.007 ± 0.002
$\delta_\perp$ [rad]	2.94 ± 0.02	2.96 ± 0.02	0.003 ± 0.005 ± 0.001

TABLE VIII. Comparison of the LHCb results assuming no S-wave component with results from previous experiments. The uncertainties are statistical and systematic, respectively.

	LHCb (no S-wave)	*BABAR* 2007 [1]	Belle 2005 [2]	CDF 2005 [3]
$\lvert A_\parallel\rvert^2$	0.220 ± 0.004 ± 0.003	0.211 ± 0.010 ± 0.006	0.231 ± 0.012 ± 0.008	0.211 ± 0.012 ± 0.009
$\lvert A_\perp\rvert^2$	0.210 ± 0.004 ± 0.004	0.233 ± 0.010 ± 0.005	0.195 ± 0.012 ± 0.008	0.220 ± 0.015 ± 0.012
$\delta_\parallel$ [rad]	−2.98 ± 0.03 ± 0.01	−2.93 ± 0.08 ± 0.04	−2.887 ± 0.090 ± 0.008	−2.97 ± 0.08 ± 0.03
$\delta_\perp$ [rad]	2.97 ± 0.02 ± 0.02	2.91 ± 0.05 ± 0.03	2.938 ± 0.064 ± 0.010	2.97 ± 0.06 ± 0.01

single bin in $m(K^+\pi^-)$, and no S-wave component has been included. To allow comparison with recent results, the fit is repeated in a single $m(K^+\pi^-)$ bin with the S-wave component set to zero. The results are summarized in Table VIII and are consistent with the previous results, and they are more accurate by a factor of 2 to 3. *BABAR* has also resolved the twofold ambiguity in the strong phases [30,33] but has not reported S-wave fractions in separate bins.

VIII. CONCLUSION

A full angular analysis of the decay $B^0 \to J/\psi K^{*0}$ has been performed. The polarization amplitudes and their strong phases are measured using data, corresponding to an integrated luminosity of 1.0 fb^{-1}, collected in pp collisions at a center-of-mass energy of 7 TeV with the LHCb detector. The results are consistent with previous measurements and confirm the theoretical predictions mentioned in Sec. I. The ambiguity in the strong phases is resolved by measuring the relative S- and P-wave phases in bins of the $K^+\pi^-$ invariant mass. No significant direct CP asymmetry is observed.

ACKNOWLEDGMENTS

We express our gratitude to our colleagues in the CERN accelerator departments for the excellent performance of the LHC. We thank the technical and administrative staff at the LHCb institutes. We acknowledge support from CERN and from the national agencies: CAPES, CNPq, FAPERJ and FINEP (Brazil); NSFC (China); CNRS/IN2P3 and Region Auvergne (France); BMBF, DFG, HGF and MPG (Germany); SFI (Ireland); INFN (Italy); FOM and NWO (The Netherlands); SCSR (Poland); MEN/IFA (Romania); MinES, Rosatom, RFBR and NRC ''Kurchatov Institute'' (Russia); MinECo, XuntaGal and GENCAT (Spain); SNSF and SER

(Switzerland); NAS Ukraine (Ukraine); STFC (United Kingdom); NSF (USA). We also acknowledge the support received from the ERC under FP7. The Tier1 computing centers are supported by IN2P3 (France), KIT and BMBF (Germany), INFN (Italy), NWO and SURF (The Netherlands), PIC (Spain), GridPP (United Kingdom). We are thankful for the computing resources put at our disposal by Yandex LLC (Russia), as well as to the communities behind the multiple open source software packages that we depend on.

[1] B. Aubert *et al.* (*BABAR* Collaboration), Phys. Rev. D **76**, 031102 (2007).
[2] R. Itoh *et al.* (Belle Collaboration), Phys. Rev. Lett. **95**, 091601 (2005).
[3] F. Abe *et al.* (CDF Collaboration), CDF 8950, 2007.
[4] R. Aleksan, A. Le Yaouanc, L. Oliver, O. Pène, and J.-C. Raynal, Phys. Rev. D **51**, 6235 (1995).
[5] D. Melikhov and B. Stech, Phys. Rev. D **62**, 014006 (2000).
[6] H. Cheng, Y. Keum, and K. Yang, Int. J. Mod. Phys. A **18**, 1437 (2003).
[7] D. London, N. Sinha, and R. Sinha, Europhys. Lett. **67**, 579 (2004).
[8] X.-G. He and W.-S. Hou, Phys. Rev. D **58**, 117502 (1998).
[9] W.-S. Hou, M. Nagashima, and A. Soddu, Phys. Rev. D **71**, 016007 (2005).
[10] D. London, N. Sinha, and R. Sinha, arXiv:hep-ph/0207007v1.
[11] M. Gronau and J. L. Rosner, Phys. Lett. B **669**, 321 (2008).
[12] K. Abe *et al.* (Belle Collaboration), Phys. Lett. B **538**, 11 (2002).
[13] R. Aaij *et al.* (LHCb Collaboration), Phys. Rev. D **87**, 072004 (2013).
[14] R. Aaij *et al.* (LHCb Collaboration), Phys. Rev. D **87**, 112010 (2013).
[15] Y. Xie, P. Clarke, G. Cowan, and F. Muheim, J. High Energy Phys. 09 (2009) 074.
[16] B. Adeva *et al.* (LHCb Collaboration), arXiv:0912.4179.
[17] A. A. Alves, Jr. *et al.* (LHCb Collaboration), JINST **3**, S08005 (2008).
[18] M. Adinolfi *et al.*, Eur. Phys. J. C **73**, 2431 (2013).
[19] T. Sjostrand, S. Mrenna, and P. Z. Skands, J. High Energy Phys. 05 (2006) 026.
[20] I. Belyaev *et al.*, *Nuclear Science Symposium Conference Record (NSS/MIC)* (IEEE, New York, 2010), p. 1155.
[21] D. Lange, Nucl. Instrum. Methods Phys. Res., Sect. A **462**, 152 (2001).
[22] P. Golonka and Z. Was, Eur. Phys. J. C **45**, 97 (2006).
[23] J. Allison *et al.* (GEANT4 Collaboration), IEEE Trans. Nucl. Sci. **53**, 270 (2006); S. Agostinelli *et al.* (GEANT4 Collaboration), Nucl. Instrum. Methods Phys. Res., Sect. A **506**, 250 (2003).
[24] M. Clemencic, G. Corti, S. Easo, C. R. Jones, S. Miglioranzi, M. Pappagallo, and P. Robbe, J. Phys. Conf. Ser. **331**, 032023 (2011).
[25] R. Aaij *et al.* (LHCb Collaboration), JINST **8**, P04022 (2013).
[26] J. Beringer *et al.* (Particle Data Group), Phys. Rev. D **86**, 010001 (2012).
[27] W. D. Hulsbergen, Nucl. Instrum. Methods Phys. Res., Sect. A **552**, 566 (2005).
[28] M. Pivk and F. R. Le Diberder, Nucl. Instrum. Methods Phys. Res., Sect. A **555**, 356 (2005).
[29] R. Aaij *et al.* (LHCb Collaboration), Phys. Lett. B **709**, 177 (2012).
[30] B. Aubert *et al.* (*BABAR* Collaboration), Phys. Rev. D **71**, 032005 (2005).
[31] R. Aaij *et al.* (LHCb Collaboration), Phys. Rev. Lett. **108**, 241801 (2012).
[32] R. Aaij *et al.* (LHCb Collaboration), Phys. Rev. D **86**, 071102 (2012).
[33] B. Aubert *et al.* (*BABAR* Collaboration), Phys. Rev. Lett. **87**, 241801 (2001).

R. Aaij,[40] C. Abellan Beteta,[35,n] B. Adeva,[36] M. Adinolfi,[45] C. Adrover,[6] A. Affolder,[51] Z. Ajaltouni,[5] J. Albrecht,[9] F. Alessio,[37] M. Alexander,[50] S. Ali,[40] G. Alkhazov,[29] P. Alvarez Cartelle,[36] A. A. Alves, Jr.,[24,37] S. Amato,[2] S. Amerio,[21] Y. Amhis,[7] L. Anderlini,[17,f] J. Anderson,[39] R. Andreassen,[56] R. B. Appleby,[53] O. Aquines Gutierrez,[10] F. Archilli,[18] A. Artamonov,[34] M. Artuso,[58] E. Aslanides,[6] G. Auriemma,[24,m] S. Bachmann,[11] J. J. Back,[47] C. Baesso,[59] V. Balagura,[30] W. Baldini,[16] R. J. Barlow,[53] C. Barschel,[37] S. Barsuk,[7] W. Barter,[46] Th. Bauer,[40] A. Bay,[38] J. Beddow,[50] F. Bedeschi,[22] I. Bediaga,[1] S. Belogurov,[30] K. Belous,[34] I. Belyaev,[30] E. Ben-Haim,[8] G. Bencivenni,[18] S. Benson,[49] J. Benton,[45] A. Berezhnoy,[31] R. Bernet,[39] M.-O. Bettler,[46] M. van Beuzekom,[40] A. Bien,[11] S. Bifani,[44] T. Bird,[53] A. Bizzeti,[17,h] P. M. Bjørnstad,[53] T. Blake,[37] F. Blanc,[38] J. Blouw,[11] S. Blusk,[58] V. Bocci,[24] A. Bondar,[33] N. Bondar,[29] W. Bonivento,[15] S. Borghi,[53] A. Borgia,[58] T. J. V. Bowcock,[51] E. Bowen,[39] C. Bozzi,[16] T. Brambach,[9] J. van den Brand,[41] J. Bressieux,[38] D. Brett,[53] M. Britsch,[10] T. Britton,[58] N. H. Brook,[45] H. Brown,[51] I. Burducea,[28] A. Bursche,[39] G. Busetto,[21,p] J. Buytaert,[37] S. Cadeddu,[15] O. Callot,[7] M. Calvi,[20,j] M. Calvo Gomez,[35,n] A. Camboni,[35] P. Campana,[18,37] D. Campora Perez,[37] A. Carbone,[14,c] G. Carboni,[23,k] R. Cardinale,[19,i] A. Cardini,[15] H. Carranza-Mejia,[49] L. Carson,[52] K. Carvalho Akiba,[2] G. Casse,[51]

L. Castillo Garcia,[37] M. Cattaneo,[37] Ch. Cauet,[9] M. Charles,[54] Ph. Charpentier,[37] P. Chen,[3,38] N. Chiapolini,[39] M. Chrzaszcz,[25] K. Ciba,[37] X. Cid Vidal,[37] G. Ciezarek,[52] P. E. L. Clarke,[49] M. Clemencic,[37] H. V. Cliff,[46] J. Closier,[37] C. Coca,[28] V. Coco,[40] J. Cogan,[6] E. Cogneras,[5] P. Collins,[37] A. Comerma-Montells,[35] A. Contu,[15] A. Cook,[45] M. Coombes,[45] S. Coquereau,[8] G. Corti,[37] B. Couturier,[37] G. A. Cowan,[49] D. C. Craik,[47] S. Cunliffe,[52] R. Currie,[49] C. D'Ambrosio,[37] P. David,[8] P. N. Y. David,[40] A. Davis,[56] I. De Bonis,[4] K. De Bruyn,[40] S. De Capua,[53] M. De Cian,[39] J. M. De Miranda,[1] L. De Paula,[2] W. De Silva,[56] P. De Simone,[18] D. Decamp,[4] M. Deckenhoff,[9] L. Del Buono,[8] N. Déléage,[4] D. Derkach,[14] O. Deschamps,[5] F. Dettori,[41] A. Di Canto,[11] H. Dijkstra,[37] M. Dogaru,[28] S. Donleavy,[51] F. Dordei,[11] A. Dosil Suárez,[36] D. Dossett,[47] A. Dovbnya,[42] F. Dupertuis,[38] R. Dzhelyadin,[34] A. Dziurda,[25] A. Dzyuba,[29] S. Easo,[48,37] U. Egede,[52] V. Egorychev,[30] S. Eidelman,[33] D. van Eijk,[40] S. Eisenhardt,[49] U. Eitschberger,[9] R. Ekelhof,[9] L. Eklund,[50,37] I. El Rifai,[5] Ch. Elsasser,[39] D. Elsby,[44] A. Falabella,[14,e] C. Färber,[11] G. Fardell,[49] C. Farinelli,[40] S. Farry,[51] V. Fave,[38] D. Ferguson,[49] V. Fernandez Albor,[36] F. Ferreira Rodrigues,[1] M. Ferro-Luzzi,[37] S. Filippov,[32] M. Fiore,[16] C. Fitzpatrick,[37] M. Fontana,[10] F. Fontanelli,[19,l] R. Forty,[37] O. Francisco,[2] M. Frank,[37] C. Frei,[37] M. Frosini,[17,f] S. Furcas,[20] E. Furfaro,[23,k] A. Gallas Torreira,[36] D. Galli,[14,c] M. Gandelman,[2] P. Gandini,[58] Y. Gao,[3] J. Garofoli,[58] P. Garosi,[53] J. Garra Tico,[46] L. Garrido,[35] C. Gaspar,[37] R. Gauld,[54] E. Gersabeck,[11] M. Gersabeck,[53] T. Gershon,[47,37] Ph. Ghez,[4] V. Gibson,[46] V. V. Gligorov,[37] C. Göbel,[59] D. Golubkov,[30] A. Golutvin,[52,30,37] A. Gomes,[2] H. Gordon,[54] M. Grabalosa Gándara,[5] R. Graciani Diaz,[35] L. A. Granado Cardoso,[37] E. Graugés,[35] G. Graziani,[17] A. Grecu,[28] E. Greening,[54] S. Gregson,[46] P. Griffith,[44] O. Grünberg,[60] B. Gui,[58] E. Gushchin,[32] Yu. Guz,[34,37] T. Gys,[37] C. Hadjivasiliou,[58] G. Haefeli,[38] C. Haen,[37] S. C. Haines,[46] S. Hall,[52] T. Hampson,[45] S. Hansmann-Menzemer,[11] N. Harnew,[54] S. T. Harnew,[45] J. Harrison,[53] T. Hartmann,[60] J. He,[37] V. Heijne,[40] K. Hennessy,[51] P. Henrard,[5] J. A. Hernando Morata,[36] E. van Herwijnen,[37] A. Hicheur,[1] E. Hicks,[51] D. Hill,[54] M. Hoballah,[5] C. Hombach,[53] P. Hopchev,[4] W. Hulsbergen,[40] P. Hunt,[54] T. Huse,[51] N. Hussain,[54] D. Hutchcroft,[51] D. Hynds,[50] V. Iakovenko,[43] M. Idzik,[26] P. Ilten,[12] R. Jacobsson,[37] A. Jaeger,[11] E. Jans,[40] P. Jaton,[38] A. Jawahery,[57] F. Jing,[3] M. John,[54] D. Johnson,[54] C. R. Jones,[46] C. Joram,[37] B. Jost,[37] M. Kaballo,[9] S. Kandybei,[42] M. Karacson,[37] T. M. Karbach,[37] I. R. Kenyon,[44] U. Kerzel,[37] T. Ketel,[41] A. Keune,[38] B. Khanji,[20] O. Kochebina,[7] I. Komarov,[38] R. F. Koopman,[41] P. Koppenburg,[40] M. Korolev,[31] A. Kozlinskiy,[40] L. Kravchuk,[32] K. Kreplin,[11] M. Kreps,[47] G. Krocker,[11] P. Krokovny,[33] F. Kruse,[9] M. Kucharczyk,[20,25,j] V. Kudryavtsev,[33] T. Kvaratskheliya,[30,37] V. N. La Thi,[38] D. Lacarrere,[37] G. Lafferty,[53] A. Lai,[15] D. Lambert,[49] R. W. Lambert,[41] E. Lanciotti,[37] G. Lanfranchi,[18,37] C. Langenbruch,[37] T. Latham,[47] C. Lazzeroni,[44] R. Le Gac,[6] J. van Leerdam,[40] J.-P. Lees,[4] R. Lefèvre,[5] A. Leflat,[31] J. Lefrançois,[7] S. Leo,[22] O. Leroy,[6] T. Lesiak,[25] B. Leverington,[11] Y. Li,[3] L. Li Gioi,[5] M. Liles,[51] R. Lindner,[37] C. Linn,[11] B. Liu,[3] G. Liu,[37] S. Lohn,[37] I. Longstaff,[50] J. H. Lopes,[2] E. Lopez Asamar,[35] N. Lopez-March,[38] H. Lu,[3] D. Lucchesi,[21,p] J. Luisier,[38] H. Luo,[49] F. Machefert,[7] I. V. Machikhiliyan,[4,30] F. Maciuc,[28] O. Maev,[29,37] S. Malde,[54] G. Manca,[15,d] G. Mancinelli,[6] U. Marconi,[14] R. Märki,[38] J. Marks,[11] G. Martellotti,[24] A. Martens,[8] A. Martín Sánchez,[7] M. Martinelli,[40] D. Martinez Santos,[41] D. Martins Tostes,[2] A. Massafferri,[1] R. Matev,[37] Z. Mathe,[37] C. Matteuzzi,[20] E. Maurice,[6] A. Mazurov,[16,32,37,e] B. Mc Skelly,[51] J. McCarthy,[44] A. McNab,[53] R. McNulty,[12] B. Meadows,[56,54] F. Meier,[9] M. Meissner,[11] M. Merk,[40] D. A. Milanes,[8] M.-N. Minard,[4] J. Molina Rodriguez,[59] S. Monteil,[5] D. Moran,[53] P. Morawski,[25] M. J. Morello,[22,r] R. Mountain,[58] I. Mous,[40] F. Muheim,[49] K. Müller,[39] R. Muresan,[28] B. Muryn,[26] B. Muster,[38] P. Naik,[45] T. Nakada,[38] R. Nandakumar,[48] I. Nasteva,[1] M. Needham,[49] N. Neufeld,[37] A. D. Nguyen,[38] T. D. Nguyen,[38] C. Nguyen-Mau,[38,o] M. Nicol,[7] V. Niess,[5] R. Niet,[9] N. Nikitin,[31] T. Nikodem,[11] A. Nomerotski,[54] A. Novoselov,[34] A. Oblakowska-Mucha,[26] V. Obraztsov,[34] S. Oggero,[40] S. Ogilvy,[50] O. Okhrimenko,[43] R. Oldeman,[15,d] M. Orlandea,[28] J. M. Otalora Goicochea,[2] P. Owen,[52] A. Oyanguren,[35] B. K. Pal,[58] A. Palano,[13,b] M. Palutan,[18] J. Panman,[37] A. Papanestis,[48] M. Pappagallo,[50] C. Parkes,[53] C. J. Parkinson,[52] G. Passaleva,[17] G. D. Patel,[51] M. Patel,[52] G. N. Patrick,[48] C. Patrignani,[19,i] C. Pavel-Nicorescu,[28] A. Pazos Alvarez,[36] A. Pellegrino,[40] G. Penso,[24,l] M. Pepe Altarelli,[37] S. Perazzini,[14,c] D. L. Perego,[20,j] E. Perez Trigo,[36] A. Pérez-Calero Yzquierdo,[35] P. Perret,[5] M. Perrin-Terrin,[6] G. Pessina,[20] K. Petridis,[52] A. Petrolini,[19,i] A. Phan,[58] E. Picatoste Olloqui,[35] B. Pietrzyk,[4] T. Pilař,[47] D. Pinci,[24] S. Playfer,[49] M. Plo Casasus,[36] F. Polci,[8] G. Polok,[25] A. Poluektov,[47,33] E. Polycarpo,[2] A. Popov,[34] D. Popov,[10] B. Popovici,[28] C. Potterat,[35] A. Powell,[54] J. Prisciandaro,[38] A. Pritchard,[51] C. Prouve,[7] V. Pugatch,[43] A. Puig Navarro,[38] G. Punzi,[22,q] W. Qian,[4] J. H. Rademacker,[45] B. Rakotomiaramanana,[38] M. S. Rangel,[2] I. Raniuk,[42] N. Rauschmayr,[37] G. Raven,[41] S. Redford,[54] M. M. Reid,[47] A. C. dos Reis,[1] S. Ricciardi,[48] A. Richards,[52] K. Rinnert,[51] V. Rives Molina,[35] D. A. Roa Romero,[5] P. Robbe,[7] E. Rodrigues,[53] P. Rodriguez Perez,[36] S. Roiser,[37] V. Romanovsky,[34] A. Romero Vidal,[36] J. Rouvinet,[38] T. Ruf,[37] F. Ruffini,[22]

H. Ruiz,[35] P. Ruiz Valls,[35] G. Sabatino,[24,k] J. J. Saborido Silva,[36] N. Sagidova,[29] P. Sail,[50] B. Saitta,[15,d] V. Salustino Guimaraes,[2] C. Salzmann,[39] B. Sanmartin Sedes,[36] M. Sannino,[19,i] R. Santacesaria,[24] C. Santamarina Rios,[36] E. Santovetti,[23,k] M. Sapunov,[6] A. Sarti,[18,l] C. Satriano,[24,m] A. Satta,[23] M. Savrie,[16,e] D. Savrina,[30,31] P. Schaack,[52] M. Schiller,[41] H. Schindler,[37] M. Schlupp,[9] M. Schmelling,[10] B. Schmidt,[37] O. Schneider,[38] A. Schopper,[37] M.-H. Schune,[7] R. Schwemmer,[37] B. Sciascia,[18] A. Sciubba,[24] M. Seco,[36] A. Semennikov,[30] K. Senderowska,[26] I. Sepp,[52] N. Serra,[39] J. Serrano,[6] P. Seyfert,[11] M. Shapkin,[34] I. Shapoval,[16,42] P. Shatalov,[30] Y. Shcheglov,[29] T. Shears,[51,37] L. Shekhtman,[33] O. Shevchenko,[42] V. Shevchenko,[30] A. Shires,[52] R. Silva Coutinho,[47] T. Skwarnicki,[58] N. A. Smith,[51] E. Smith,[54,48] M. Smith,[53] M. D. Sokoloff,[56] F. J. P. Soler,[50] F. Soomro,[18] D. Souza,[45] B. Souza De Paula,[2] B. Spaan,[9] A. Sparkes,[49] P. Spradlin,[50] F. Stagni,[37] S. Stahl,[11] O. Steinkamp,[39] S. Stoica,[28] S. Stone,[58] B. Storaci,[39] M. Straticiuc,[28] U. Straumann,[39] V. K. Subbiah,[37] L. Sun,[56] S. Swientek,[9] V. Syropoulos,[41] M. Szczekowski,[27] P. Szczypka,[38,37] T. Szumlak,[26] S. T'Jampens,[4] M. Teklishyn,[7] E. Teodorescu,[28] F. Teubert,[37] C. Thomas,[54] E. Thomas,[37] J. van Tilburg,[11] V. Tisserand,[4] M. Tobin,[38] S. Tolk,[41] D. Tonelli,[37] S. Topp-Joergensen,[54] N. Torr,[54] E. Tournefier,[4,52] S. Tourneur,[38] M. T. Tran,[38] M. Tresch,[39] A. Tsaregorodtsev,[6] P. Tsopelas,[40] N. Tuning,[40] M. Ubeda Garcia,[37] A. Ukleja,[27] D. Urner,[53] U. Uwer,[11] V. Vagnoni,[14] G. Valenti,[14] R. Vazquez Gomez,[35] P. Vazquez Regueiro,[36] S. Vecchi,[16] J. J. Velthuis,[45] M. Veltri,[17,g] G. Veneziano,[38] M. Vesterinen,[37] B. Viaud,[7] D. Vieira,[2] X. Vilasis-Cardona,[35,n] A. Vollhardt,[39] D. Volyanskyy,[10] D. Voong,[45] A. Vorobyev,[29] V. Vorobyev,[33] C. Voß,[60] H. Voss,[10] R. Waldi,[60] R. Wallace,[12] S. Wandernoth,[11] J. Wang,[58] D. R. Ward,[46] N. K. Watson,[44] A. D. Webber,[53] D. Websdale,[52] M. Whitehead,[47] J. Wicht,[37] J. Wiechczynski,[25] D. Wiedner,[11] L. Wiggers,[40] G. Wilkinson,[54] M. P. Williams,[47,48] M. Williams,[55] F. F. Wilson,[48] J. Wishahi,[9] M. Witek,[25] S. A. Wotton,[46] S. Wright,[46] S. Wu,[3] K. Wyllie,[37] Y. Xie,[49,37] Z. Xing,[58] Z. Yang,[3] R. Young,[49] X. Yuan,[3] O. Yushchenko,[34] M. Zangoli,[14] M. Zavertyaev,[10,a] F. Zhang,[3] L. Zhang,[58] W. C. Zhang,[12] Y. Zhang,[3] A. Zhelezov,[11] A. Zhokhov,[30] L. Zhong,[3] and A. Zvyagin[37]

(LHCb Collaboration)

[1]*Centro Brasileiro de Pesquisas Físicas (CBPF), Rio de Janeiro, Brazil*
[2]*Universidade Federal do Rio de Janeiro (UFRJ), Rio de Janeiro, Brazil*
[3]*Center for High Energy Physics, Tsinghua University, Beijing, China*
[4]*LAPP, Université de Savoie, CNRS/IN2P3, Annecy-Le-Vieux, France*
[5]*Clermont Université, Université Blaise Pascal, CNRS/IN2P3, LPC, Clermont-Ferrand, France*
[6]*CPPM, Aix-Marseille Université, CNRS/IN2P3, Marseille, France*
[7]*LAL, Université Paris-Sud, CNRS/IN2P3, Orsay, France*
[8]*LPNHE, Université Pierre et Marie Curie, Université Paris Diderot, CNRS/IN2P3, Paris, France*
[9]*Fakultät Physik, Technische Universität Dortmund, Dortmund, Germany*
[10]*Max-Planck-Institut für Kernphysik (MPIK), Heidelberg, Germany*
[11]*Physikalisches Institut, Ruprecht-Karls-Universität Heidelberg, Heidelberg, Germany*
[12]*School of Physics, University College Dublin, Dublin, Ireland*
[13]*Sezione INFN di Bari, Bari, Italy*
[14]*Sezione INFN di Bologna, Bologna, Italy*
[15]*Sezione INFN di Cagliari, Cagliari, Italy*
[16]*Sezione INFN di Ferrara, Ferrara, Italy*
[17]*Sezione INFN di Firenze, Firenze, Italy*
[18]*Laboratori Nazionali dell'INFN di Frascati, Frascati, Italy*
[19]*Sezione INFN di Genova, Genova, Italy*
[20]*Sezione INFN di Milano Bicocca, Milano, Italy*
[21]*Sezione INFN di Padova, Padova, Italy*
[22]*Sezione INFN di Pisa, Pisa, Italy*
[23]*Sezione INFN di Roma Tor Vergata, Roma, Italy*
[24]*Sezione INFN di Roma La Sapienza, Roma, Italy*
[25]*Henryk Niewodniczanski Institute of Nuclear Physics Polish Academy of Sciences, Kraków, Poland*
[26]*Faculty of Physics and Applied Computer Science, AGH - University of Science and Technology, Kraków, Poland*
[27]*National Center for Nuclear Research (NCBJ), Warsaw, Poland*
[28]*Horia Hulubei National Institute of Physics and Nuclear Engineering, Bucharest-Magurele, Romania*
[29]*Petersburg Nuclear Physics Institute (PNPI), Gatchina, Russia*
[30]*Institute of Theoretical and Experimental Physics (ITEP), Moscow, Russia*
[31]*Institute of Nuclear Physics, Moscow State University (SINP MSU), Moscow, Russia*

[32]*Institute for Nuclear Research of the Russian Academy of Sciences (INR RAN), Moscow, Russia*
[33]*Budker Institute of Nuclear Physics (SB RAS) and Novosibirsk State University, Novosibirsk, Russia*
[34]*Institute for High Energy Physics (IHEP), Protvino, Russia*
[35]*Universitat de Barcelona, Barcelona, Spain*
[36]*Universidad de Santiago de Compostela, Santiago de Compostela, Spain*
[37]*European Organization for Nuclear Research (CERN), Geneva, Switzerland*
[38]*Ecole Polytechnique Fédérale de Lausanne (EPFL), Lausanne, Switzerland*
[39]*Physik-Institut, Universität Zürich, Zürich, Switzerland*
[40]*Nikhef National Institute for Subatomic Physics, Amsterdam, The Netherlands*
[41]*Nikhef National Institute for Subatomic Physics and VU University Amsterdam, Amsterdam, The Netherlands*
[42]*NSC Kharkiv Institute of Physics and Technology (NSC KIPT), Kharkiv, Ukraine*
[43]*Institute for Nuclear Research of the National Academy of Sciences (KINR), Kyiv, Ukraine*
[44]*University of Birmingham, Birmingham, United Kingdom*
[45]*H.H. Wills Physics Laboratory, University of Bristol, Bristol, United Kingdom*
[46]*Cavendish Laboratory, University of Cambridge, Cambridge, United Kingdom*
[47]*Department of Physics, University of Warwick, Coventry, United Kingdom*
[48]*STFC Rutherford Appleton Laboratory, Didcot, United Kingdom*
[49]*School of Physics and Astronomy, University of Edinburgh, Edinburgh, United Kingdom*
[50]*School of Physics and Astronomy, University of Glasgow, Glasgow, United Kingdom*
[51]*Oliver Lodge Laboratory, University of Liverpool, Liverpool, United Kingdom*
[52]*Imperial College London, London, United Kingdom*
[53]*School of Physics and Astronomy, University of Manchester, Manchester, United Kingdom*
[54]*Department of Physics, University of Oxford, Oxford, United Kingdom*
[55]*Massachusetts Institute of Technology, Cambridge, Massachusetts, USA*
[56]*University of Cincinnati, Cincinnati, Ohio, USA*
[57]*University of Maryland, College Park, Maryland, USA*
[58]*Syracuse University, Syracuse, New York, USA*
[59]*Pontifícia Universidade Católica do Rio de Janeiro (PUC-Rio), Rio de Janeiro, Brazil and Universidade Federal do Rio de Janeiro (UFRJ), Rio de Janeiro, Brazil*
[60]*Institut für Physik, Universität Rostock, Rostock, Germany and Physikalisches Institut, Ruprecht-Karls-Universität Heidelberg, Heidelberg, Germany*

[a]Also at P.N. Lebedev Physical Institute, Russian Academy of Science (LPI RAS), Moscow, Russia.
[b]Also at Università di Bari, Bari, Italy.
[c]Also at Università di Bologna, Bologna, Italy.
[d]Also at Università di Cagliari, Cagliari, Italy.
[e]Also at Università di Ferrara, Ferrara, Italy.
[f]Also at Università di Firenze, Firenze, Italy.
[g]Also at Università di Urbino, Urbino, Italy.
[h]Also at Università di Modena e Reggio Emilia, Modena, Italy.
[i]Also at Università di Genova, Genova, Italy.
[j]Also at Università di Milano Bicocca, Milano, Italy.
[k]Also at Università di Roma Tor Vergata, Roma, Italy.
[l]Also at Università di Roma La Sapienza, Roma, Italy.
[m]Also at Università della Basilicata, Potenza, Italy.
[n]Also at LIFAELS, La Salle, Universitat Ramon Llull, Barcelona, Spain.
[o]Also at Hanoi University of Science, Hanoi, Vietnam.
[p]Also at Università di Padova, Padova, Italy.
[q]Also at Università di Pisa, Pisa, Italy.
[r]Also at Scuola Normale Superiore, Pisa, Italy.